Two-dimensional turbulence in three-dimensional flows

H. Xia[a] and N. Francois
Research School of Physics and Engineering, The Australian National University, Canberra, ACT 2601, Australia

(Received 9 April 2017; accepted 17 August 2017; published online 11 September 2017)

This paper presents a review of experiments performed in three-dimensional flows that show behaviour associated with two-dimensional turbulence. Experiments reveal the presence of the inverse energy cascade in two different systems, namely, flows in thick fluid layers driven electromagnetically and the Faraday wave driven flows. In thick fluid layers, large-scale coherent structures can shear off the vertical eddies and reinforce the planarity of the flow. Such structures are either self-generated or externally imposed. In the Faraday wave driven flows, a seemingly three-dimensional flow is shown to be actually two-dimensional when it is averaged over several Faraday wave periods. In this system, a coupling between the wave motion and 2D hydrodynamic turbulence is uncovered. *Published by AIP Publishing.* [http://dx.doi.org/10.1063/1.5000863]

I. INTRODUCTION

Considering an idealized two-dimensional (2D) fluid, Kraichnan predicted that energy flows towards small wave numbers when turbulence is forced at some intermediate wave number k_f.[1] This transfer of spectral energy towards large scales was named the *inverse* cascade of energy. When 2D turbulence is spatially confined, the spectral energy accumulates at the box size and large-scale vortices are formed. This phenomenon is referred to as spectral condensation.[1] While the inverse energy cascade and the spectral condensation have been confirmed in ideal numerical simulations,[2–7] one can ask the question: Is it possible to create the inverse cascade and the spectral condensation in experiments?

The first attempts to answer this question aimed at generating flows in a very thin layer of fluid. It seems logical to think that the thinner the fluid layer, the better is the prospect to obtain quasi-2D flows. This principle has inspired numerous experiments based on electromagnetically driven flows in conducting fluids[8–17] or exploring the hydrodynamical properties of soap films.[18–22] Although the approach sounds simple, it triggers a lot of challenging questions: How thin should the fluid layer be? How flat should the liquid surface remain?

Paradoxically, during the past ten years, experimental studies have shown that 2D turbulence actually exists in seemingly unfavourable configurations. Two of the most striking examples are flows generated in thick fluid layers and flows at a liquid surface perturbed by Faraday waves, both reviewed here.

In a thick layer of fluid, the flow is generally three-dimensional (3D). However, it can show features of 2D turbulence close to a fluid surface if the latter remains flat.[23] This thin layer of 2D turbulence is capable of condensing when it is bounded. The condensation can then enforce the flow two-dimensionality over the entire fluid thickness.[24] A similar phenomenology is observed when a large-scale flow is externally imposed on a 3D flow in a thick layer.[24]

A surface perturbed by Faraday waves produces flows that can be visualised with floating particles; surprisingly the motion of these floating tracers reproduces remarkably well properties of 2D turbulence.[25–29] This discovery has greatly improved the capacity of experimental modeling of 2D turbulence. For instance, the combination of electromagnetically driven and wave driven turbulent flows has widened the range of forcing scale and flow kinetic energy achievable. Experiments have been performed combining the two methods to revisit the single-particle dispersion and explore topological aspects of 2D disordered and fully turbulent flows.[30–33]

In this paper, we review experimental results obtained in the electromagnetically driven and Faraday wave driven turbulence with an emphasis on the existence of the inverse cascade in seemingly 3D systems. A comprehensive review on 2D turbulence can be found in Ref. 34. The interaction of the energy cascade with large-scale structures generated through spectral condensation or externally imposed is discussed. We also present some connections recently uncovered between wave physics and 2D hydrodynamic turbulence. These discoveries extend the domain of applications of Kraichnan's seminal ideas on 2D turbulence.

II. EXPERIMENTAL SETUPS

Electromagnetically driven turbulence [EMT, Fig. 1(a)] is produced in layers of electrolyte (Na_2SO_4 water solution) by running electric current across a fluid cell (square container 30×30 cm) placed above an array of permanent magnets.[14,15,24] The Lorenz force produces horizontal vortices that interact with each other generating complex flows. By changing the current density, one can control the degree of turbulence development. The energy is injected into the flow at a scale, the forcing scale L_f, which is approximately equal to the distance between the magnets. Two configurations can be employed in the EMT experiments: (1) a single layer of electrolyte flowing upon a solid bottom and (2) a double-layer configuration:

[a]hua.xia@anu.edu.au

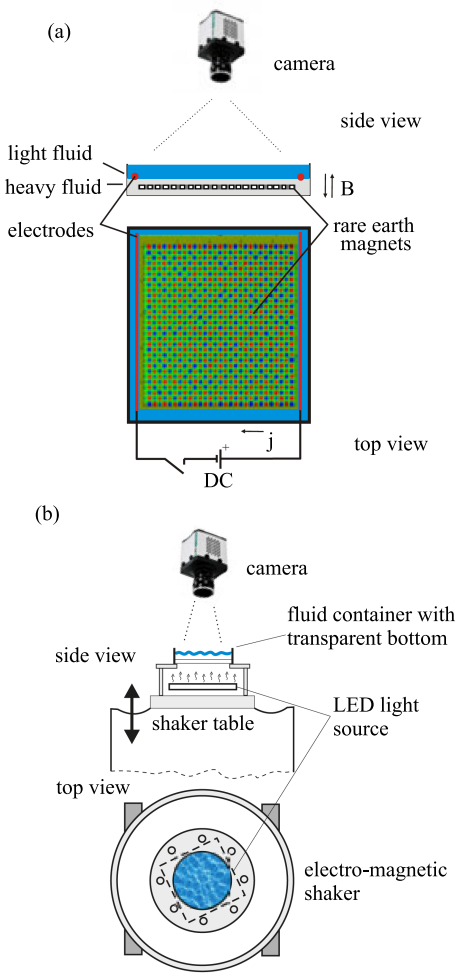

FIG. 1. Experimental setups for (a) electromagnetically driven turbulence (EMT) and (b) Faraday wave driven turbulence (FWT).

a layer of electrolyte is placed on top of a layer of denser (specific gravity $SG = 1.8$), non-conducting low-viscosity fluid (FC-3283). In this case, flows are studied in the upper layer that *slips* on the lower one. This configuration greatly reduces the dissipation related to the solid bottom wall of the container (an intrinsic 3D effect).

The experimental setup of the Faraday wave driven turbulence (FWT) is shown in Fig. 1(b). Faraday waves are generated in a container filled with water up to its brim. The water depth is 30 mm and care was taken that the liquid contact line was pinned to the edge of the container, i.e., there is no meniscus. The container is shaken vertically. The vertical oscillation is monochromatic with a frequency fixed in the range f_s = (30–110) Hz and a peak-to-peak vertical acceleration a in the range $a = (0.1–3)g$, where g is the gravitational acceleration. Above a given acceleration threshold, Faraday waves are parametrically excited at half the shaking frequency. The waves are modulationally unstable and the surface circular ripples quickly disintegrate into an assembly of oscillating solitons or oscillons.[35,36] The oscillonic field gets more and more disordered at higher accelerations.

In both experiments, the motion of the fluid is visualised by placing a floating particle with a diameter of 50 μm or 150 μm on the water surface. The use of surfactant and plasma treatment ensures initial homogenous distribution of the tracer particles. In the EMT experiments, to visualise the 3D motion inside the flow, tracer particles are suspended in the fluid. A horizontal or vertical laser sheet is used to illuminate the flow under investigation.

The particle motion is captured by using a high-resolution fast camera (such as Andor Neo sCMOS) as described in Refs. 26 and 30. In the Faraday wave experiments, the diffusing light imaging technique is used to visualize simultaneously the surface ripples and floating tracer particles.[29] A 2% milk solution added to water provides sufficient contrast for the parametrically excited waves to be observed. The velocity fields and particle trajectories are obtained using particle image velocimetry (PIV) and particle tracking velocimetry (PTV).

The forcing mechanism in two-dimensional experiments is often a point of discussion since the Kolmogorov-Kraichnan theory of turbulence considers two-dimensional flows driven by white-in-time random force. The experimental realization of such a paradigm is obviously quite challenging. In EMT experiments, since the polarity of the magnets are predefined, there is a common belief that the forcing is highly correlated in time. To circumvent this issue, there were some attempts to generate random forcing by randomising the polarity of the current in time.[9] Later, it has been shown that even the basic configuration for EMT experiments does produce random forcing. Indeed, though the forcing vortices are initially generated at fixed positions determined by the array of permanent magnets, these vortices are then pushed around and randomised by shearing and sweeping effects.[13] In Faraday waves, the horizontal array of forcing vortices can only be observed transiently.[29] After that, the vortices are pushed around and randomised in a similar fashion to what is observed in EMT.

III. EXPERIMENTAL MODELING OF 2D TURBULENCE: AN ONGOING DISCUSSION

Early experiments aimed at approaching 2D fluid motion by confining the liquid along one of its three dimensions. One elegant example is found in experiments based on flows in soap films that are typically few microns thick.[18–20] Although the hydrodynamics of soap films is a complex subject, the versatility of this experimental setup is remarkable. For instance, decaying turbulence has been investigated in a so-called soap film channel driven by gravity,[19] while a $k^{-5/3}$ spectrum can be generated by placing rough walls on the edge of the 2D channel.[21] Recently flows in soap film channels have been used to investigate the existence of a link between the frictional drag and the spectral exponent of the velocity fluctuations.[20,21] More details about 2D turbulence in soap films can be found in detailed reviews.[22,34]

Another approach was based on generating flows in a horizontal layer of mercury.[8] This conducting liquid was placed in a vertical homogeneous magnetic field while the flow was forced by applying a spatially varying electric field. In this configuration, a 2D turbulent flow can be produced, and Kolmogorov spectra were observed as well as spectral

condensation in the bounded domain. A similar setup was developed using a thin layer of electrolytic fluid over a checkerboard array of magnets of opposite polarity.[9,10] When an electric current runs through the electrolyte, a fluid motion is generated by the Lorenz force. Although flows produced in this system show features of 2D turbulence, they remain strongly affected by dissipative and 3D effects. In that respect, it was realised that two thin layers of electrolytes of different densities can be used to reduce substantially the bottom friction.[10] A more stable configuration is actually achieved by placing a thin layer of electrolyte on top of a denser layer of a non-miscible and non-conducting fluid.[12,15,24]

In these seminal studies, the guiding principle is clear: the thinner the fluid layer, the better the prospect to realise quasi-2D turbulence. However, the results shown in this review reveal that 2D turbulence does exist in thick fluid layers. This surprising observation is actually strongly supported by the recent discovery of Faraday wave driven turbulence.

IV. 2D TURBULENCE IN THIN FLUID LAYERS: THE DOUBLE LAYER CONFIGURATION

For a thin layer of electrolyte in a double-layer configuration, the inverse energy cascade and the spectral condensation have been reported.[14,15] In these experiments, turbulence is generated electromagnetically in the upper layer of the conducting fluid whose thickness does not exceed 4 ∼ 5 mm [Fig. 1(a)]. The magnets are placed 9 mm apart, giving a forcing scale of $L_f = 9$ mm and a forcing wave number of $k_f \approx 750$ rad/m.

An example of the kinetic energy spectrum is reproduced in Fig. 2(a). The spectrum shows a power-law scaling close to $k^{-5/3}$ for $k < k_f$ for the inverse energy cascade range and close to k^{-3} for $k > k_f$ for the enstrophy range. The small peak at the small wave number represents a weak condensation at large scales which develops as a result of the low dissipation in the double-layer configuration.

The Kolmogorov flux relation is used to measure the energy flow. In homogeneous 2D turbulence, spectral energy flux is expressed via the third-order moment of the velocity structure function: $\epsilon = S_3/r = 2/3S_{3L}/r$, where $S_3 = (S_{3L} + S_{3T})/2$, $S_{3L} = \langle(\delta V_L)^3\rangle$, and $S_{3T} = \langle\delta V_L(\delta V_T)^2\rangle$, respectively. Here δV_L and δV_T are, respectively, longitudinal (L) and transverse (T) components of the velocity difference between points separated by r. Angular brackets denote space and time averaging. For 3D turbulence, the third-order structure function is $S_3 = -4/5\epsilon r$. The sign and linearity of the third-order structure function have often been used as an indication of the direction of the energy flux, hence the dimensionality. The third-order structure function measured in EMT is shown in Fig. 2(b). It uncovers the presence of an inverse energy cascade for which S_3 is a positive linear function of r, from 0.01 m to 0.04 m.

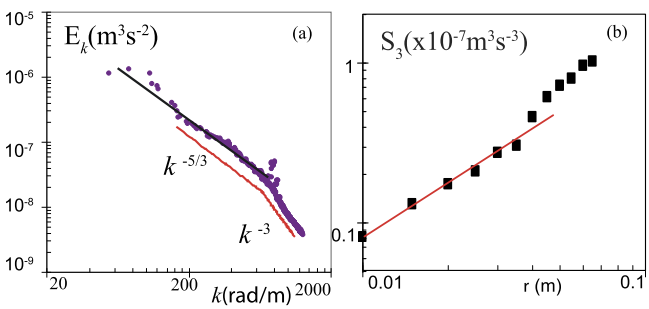

FIG. 2. (a) Kinetic energy spectra of turbulence and (b) third-order structure function measured in a double-layer EMT experiment.

It should be noted that the third-order structure function S_3 is rarely computed in experiments on 2D turbulence. One of the difficulties is related to obtaining reliable statistics, as explained in Ref. 9. Another reason is related to the presence of coherent structures, such as a spectral condensate. It is important to subtract coherent components from the instantaneous velocity fields to recover the correct statistics of the turbulent velocity fluctuations. Otherwise the velocity differences contain contributions from the spatially inhomogeneous vortex flows. Then the statistically averaged higher-order moments, or structure functions, become highly affected.

We have demonstrated that the presence of large-scale flows substantially modifies S_3 and even affects its sign.[14,15] In this case, the flow velocity and its increments contain both mean and fluctuating velocity components, $\delta V = \delta\bar{V} + \delta\tilde{V}$. The second-order structure function contains not only the second moment of velocity fluctuations $\delta\tilde{V}^2$ but also two other terms, $\langle\delta V^2\rangle = \langle\delta\bar{V}^2 + 2\delta\bar{V}\delta\tilde{V} + \delta\tilde{V}^2\rangle$. The second term averages out. The third-order moment is affected even more: $\langle\delta V^3\rangle = \langle\delta\bar{V}^3 - 3\delta\bar{V}^2\delta\tilde{V} + 3\delta\bar{V}\delta\tilde{V}^2 - \delta\tilde{V}^3\rangle$. Again, the term with $\delta\tilde{V}$ averages to zero, while the terms $\langle\delta\tilde{V}^3\rangle$ and $\langle 3\delta\bar{V}\delta\tilde{V}^2\rangle$ modify the third velocity moment due to the presence of the mean shear flow. This is also the case in situations where large coherent flows coexist with turbulence, such as in the planet atmosphere and in thick fluid layers with self-generated or externally imposed flows.[24] The effect of mean flow on the structure functions may be more complicated when the mean flow fluctuates in time and space.

V. 2D TURBULENCE IN THICK FLUID LAYERS

Real fluid layers differ from the ideal 2D model because they have finite depths and a nonzero dissipation. The effect of the layer thickness on turbulence driven by 2D forcing has been studied in 3D numerical simulations.[37] It has been shown that in "turbulence in more than two and less than three dimensions," the injected energy flux splits between a 3D direct cascade and a 2D inverse cascade. At ratios of the layer depth h over the forcing scale L_f above $h/L_f \sim 0.5$, the inverse energy cascade is greatly reduced. When the inverse energy flux is suppressed, the energy injected into the flow is transferred towards small scales by the direct cascade, developing the 3D Kolmogorov $k^{-5/3}$ spectrum at $k > k_f$. On a side note, the transition from 3D to 2D phenomenology in Rayleigh-Taylor turbulence has recently been discussed along a similar line of thought, in particular, the ratio of the width of the mixing layer to the scale of confinement was shown to be a control parameter of such a transition.[38]

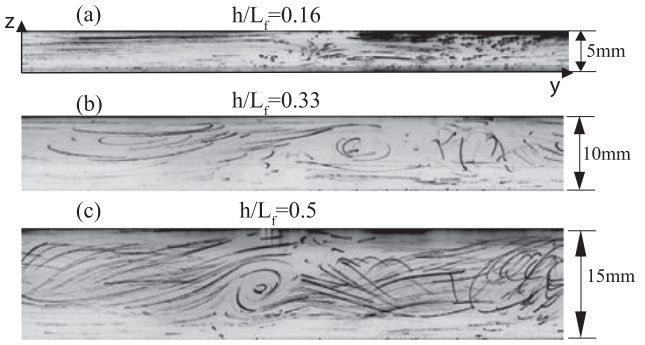

FIG. 3. The particle streaks for EMT experiments in single fluid layers of three different thicknesses (side view). (a) $h/L_f = 0.16$, (b) $h/l_f = 0.33$, and (c) $h/l_f = 0.5$. The forcing scale is 30 mm.

Physically the three-dimensionality of the flow is determined by the amount of 3D motion in the layer. This motion may naturally develop in the layer, as in Ref. 37, but it can also be injected into the flow by non-2D forcing, or it can be generated by shear-driven instabilities in the boundary layer.

Figure 3 shows particle streaks measured in experiments using a *single* fluid layer with varying thickness. In these experiments, the forcing is two-dimensional in the horizontal plane. For small h/L_f, the flow is reasonably two-dimensional. With the increase of the layer thickness, three-dimensional motions appear naturally in the layer. Note that though there is development of three-dimensional motions, there is no observation of the forward energy cascade of 3D turbulence. This is due to the low turbulence level in experiments, while numerical simulations[37] considered that inviscid fluids thus had an infinite Reynolds number.

The turbulence decay rate was proposed to be an accurate measure of the flow dimensionality.[17] In our experiments, the energy density of the flow is computed as $E = (2N^2)^{-1} \sum_i \sum_j V_{i,j}^2$, with N as the size of the 2D PIV grid on which the velocity is measured. The damping rate of the flow is estimated from the energy density decay after switching off the forcing at $t = t_0$: $E_t = E_{t_0} e^{-\alpha(t-t_0)}$. The experimentally measured decay ranges from $\alpha = 0.03\ s^{-1}$ to $0.3\ s^{-1}$ depending on the layer thickness and flow configuration.

Experiments in a single thick fluid layer show that eddy viscosity increases damping in finite-depth fluid layers compared with the quasi-2D model prediction.[17] This increase can be used to probe the flow dimensionality. For a large value of the h/L_f ratio, the increased degree of three-dimensionality leads to the suppression of the inverse energy cascade.

The situation is quite different when the dissipation at the bottom of the container is strongly reduced. Experimentally, it is achieved in the double fluid layer configuration where the lower layer consists of a dense non-conductive fluid. We conducted experiments where the top layer thickness is set to more than half the forcing scale $h/L_f \approx 0.75$.[24] Particle streaks measured in this top layer are shown in Fig. 4. At the beginning of an experiment, $t = 5$ s, 3D motion is clearly seen in the flow. As turbulence develops, $t > 5$ s, the vertical component of the particle streaks gradually decreases, and the flow becomes planar [see Figs. 4(b)–4(d)].

In the horizontal plane, at $t > 20$ s, a coherent flow develops over the entire domain[24] as shown in Figs. 5(a) and 5(b).

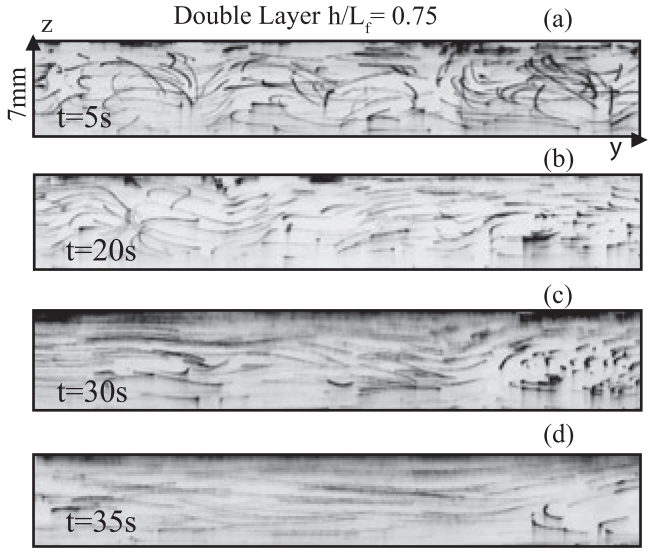

FIG. 4. Temporal evolution of the particle streaks in the top layer of thick double-layer experiments, view from the side. (a): $t = 5$ s, (b) $t = 20$ s, (c) $t = 30$ s, and (d) $t = 35$ s. $L_f = 9$ mm and $h = 7$ mm.

It signals the presence of a strong spectral condensation. The phenomenon is favoured by the low dissipation in this thick double-layer configuration. The kinetic energy spectrum at $t = 20$ s has a strong peak at the low wavenumber range, Fig. 5(c). The corresponding third-order structure, shown in Fig. 5(e), is negative and does not show any linear trend in space. As mentioned earlier, it is essential to subtract the mean flow from the calculation of any statistical descriptor when turbulence coexists with a coherent flow. The resulting mean-subtracted spectrum is shown in Fig. 5(d) and it possesses a $k^{-5/3}$ power scaling. Likewise the third-order structure function becomes a positive and linear function of space, r [Fig. 5(f)]. The observation of an inverse energy cascade in the thick fluid layer is therefore correlated with the spectral condensation of turbulence in the horizontal plane.

A similar phenomenology has been reported in a single fluid layer with an externally imposed flow.[24] Experiments were performed in a single layer of electrolyte, h = 10 mm, $L_f = 9$ mm with a much larger boundary, and L = 300 mm, to avoid spectral condensation. In this case, a large-scale vortex is imposed by using a large magnet. The timeline of the experiment is shown in Fig. 6(a) as follows:

- First, turbulence is excited.
- Then, a large vortex (150 mm diameter) is imposed on the flow by placing a magnetic dipole 2 mm above the free surface.
- Finally, the large magnet is removed and the large vortex decays, while turbulence continues to be forced.

As the magnet blocks the view, the measurements are performed during the turbulence stage and during the decay of the vortex.

The streak of fluid tracers in the y-z direction shows the presence of 3D motions in the pure turbulence regime [Fig. 6(c)]. The 3D motion is suppressed when the large magnets are placed above the liquid surface [Fig. 6(d)]. The

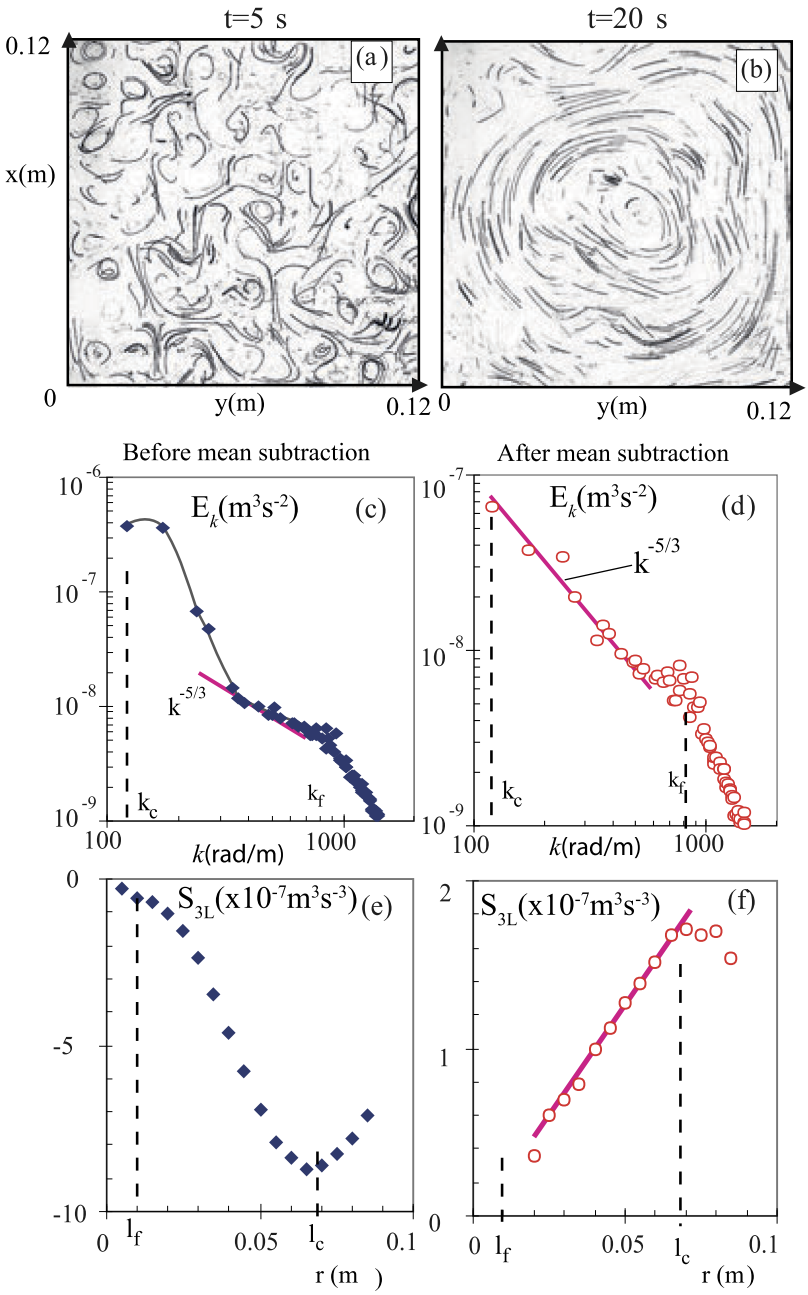

FIG. 5. Particle streak in the horizontal plane of the double-layer experiment at (a) 5 s and (b) 20 s [to be compared with Figs. 4(a) and 4(b)]. Kinetic energy spectra of the horizontal flow and the third-order structure function [(c) and (e)] before the mean subtraction and [(d) and (f)] after the mean subtraction. $l_f = 9$ mm and $h = 7$ mm. The box size is 120 mm.

flow becomes 3D again as the large-scale vortex fades away, Fig. 6(e). The kinetic energy spectra and the third-order moments have been studied. Initially (turbulence without vortex), the spectrum is substantially flatter than $k^{-5/3}$ [Fig. 6(f)]. After the large vortex is imposed, the spectrum shows a strong peak at low wave numbers. However, by using the mean subtraction, one can recover the $k^{-5/3}$ 2D inverse cascade spectrum, as shown in Fig. 6(g). The third-order moment undergoes an even more pronounced change after the imposition of the large vortex: S_3 computed after the mean subtraction is much larger than during the turbulence stage, and it becomes a positive and linear function of r over a wide range of scales, Fig. 6(h). These findings are consistent with our observation in double-layer experiments. Thus the imposed flow enforces planarity and strongly enhances the inverse energy flux.

Figure 6(b) shows results related to the turbulence energy decay measured in three different configurations: in the presence of turbulence only, of an external flow coexisting with turbulence, and of an external flow without turbulence. The decay rate of the kinetic energy is high ($\alpha = 0.3\ s^{-1}$) for the turbulence case. This is consistent with that in a single layer, where 3D motion increases dissipation through the eddy viscosity. For the large external flow, the decay rate is $\alpha = 0.09\ s^{-1}$. When the external flow coexists with turbulence, the decay rate is smaller at $\alpha = 0.06\ s^{-1}$, which suggests that the turbulence feeds the large-scale flow through the inverse energy cascade. This is a very interesting result: the large-scale vortex can secure its energy supply by suppressing vertical motions and enforcing the two-dimensionality and the inverse energy cascade.

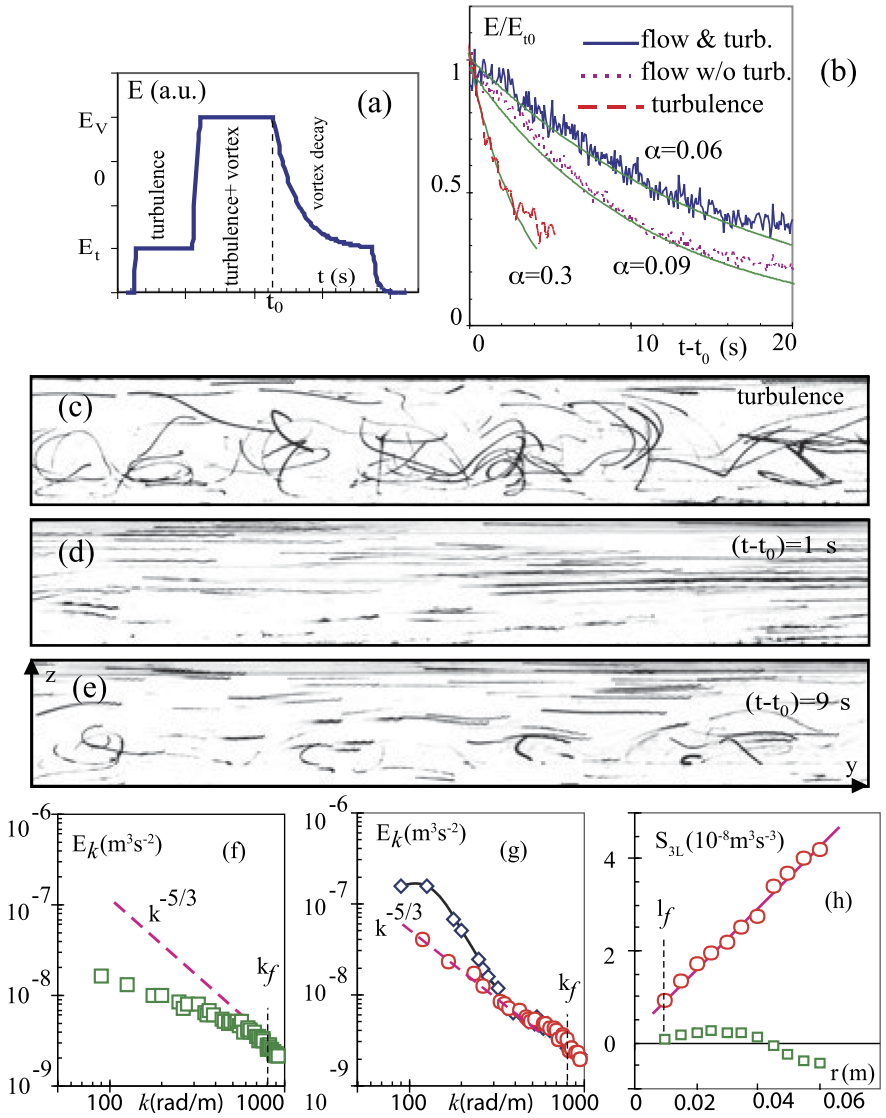

FIG. 6. (a) Timeline of the experiments showing the three stages: turbulence, turbulence + vortex, and vortex decaying with turbulence. (b) The decay of the kinetic energy of the flow in different experimental conditions: turbulence only, external flow only, and turbulence and external flow. [(c)–(e)] Vertical streaks of the fluid particles at different times of the experiments. Spectra of the single layer experiments (f) in the turbulent case and (g) in the presence of the mean flow, with (circles) and without (diamonds) the mean subtraction. (h) The third-order structure function with (circles) and without the external flow (squares). S_{3L} with the external flow case is calculated after the mean subtraction.

The observation of an inverse energy cascade in thick fluid layers is due to the strong suppression of vertical eddies in the presence of an imposed or self-generated flow.[24] The vertical shear $\Omega_s = d(V_h)/dz$ destroys vertical eddies for which the inverse turnover time is less than Ω_s.

The observation of an inverse energy cascade in thick fluid layers under the large-scale shear flow may be relevant for geophysical flows and engineering applications. An interesting example is the wavenumber spectrum of wind velocities in the Earth atmosphere measured near the tropopause,[39,40] which shows $E(k) \sim k^{-5/3}$ in the mesoscale range (10-500 km) and a strong peak at the planetary scale of 10^4 km. Numerous hypotheses have been proposed to explain the mesoscale spectrum, with most arguments centred on the direct versus the inverse energy cascade.[4,41] The shape of the spectrum alone cannot resolve this issue since both the 3D Kolmogorov direct cascade and the 2D Kraichnan inverse cascade are indistinguishable $E(k) \sim k^{-5/3}$. Direct processing of atmospheric data gave $S_3(r) < 0$ for the range of r in the mesoscales, thus favouring the direct cascade hypothesis.[42,43] However, the mesoscale turbulence in the Earth atmosphere should be affected by the large-scale flow regardless of its origin or stability, similar to the much simpler laboratory experiments. The subtraction of the mean flows, necessary for the correct flux evaluation, has not been done for the wind data. This leaves the question about the source of the mesoscale energy unresolved.

Moreover, these results may be relevant not only for thin layers but also for boundary layer flows with turbulence generated by surface roughness, convection, or other sources. *In situ* aircraft measurements in the hurricane boundary layer have recently revealed a height-dependent transition of the flow from 3D to 2D turbulence in the presence of the large-scale vortex.[44]

VI. 2D TURBULENCE IN FARADAY WAVES

Ripples that appear on the surface of a vertically vibrated liquid are known as Faraday waves. They are widely used to study a broad range of phenomena, such as pattern formation, solitons, extreme wave events, and others.[35,36,45–50] Another interesting aspect of this system is that Faraday waves produce slow horizontal flows. The dispersive behaviour of fluid tracers

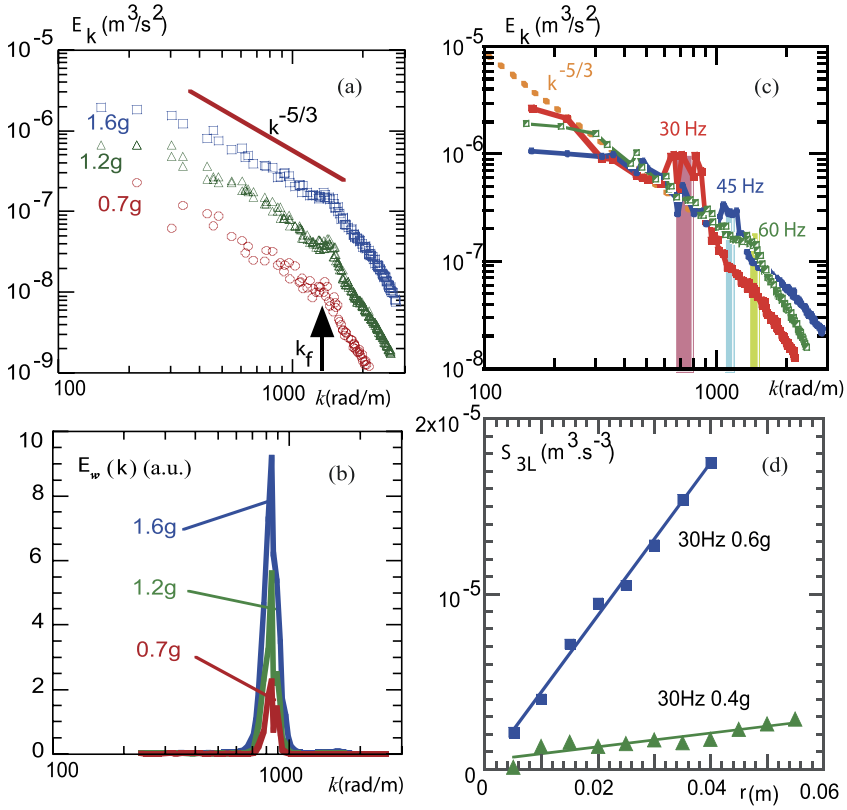

FIG. 7. (a) Wave number spectra of the kinetic energy of the horizontal flow and (b) power spectra of the surface wave elevation at f_s = 60 Hz (at three vertical accelerations $a = 0.7$, 1.2, and $1.6g$). (c) Kinetic energy spectra at different driving frequencies f_s = 30, 45, and 60 Hz. (d) Third-order structure function for two different forcing scales at a driving frequency of f_s = 30 Hz. The water depth is 30 mm and the wave height (standard deviation of the elevation field) ranges from 0.4 to 2 mm in these experiments.

on a liquid surface perturbed by those waves was investigated two decades ago in a series of seminal papers.[51–53]

It has recently been found[25,27,28] that the *horizontal* motion of floating particles on the surface of Faraday waves shows several properties consistent with the fluid motion in 2D turbulence. This turbulent horizontal transport was referred to as Faraday wave driven flows. In particular, a $k^{-5/3}$ spectrum has been reported. In the first study,[25] the experiments

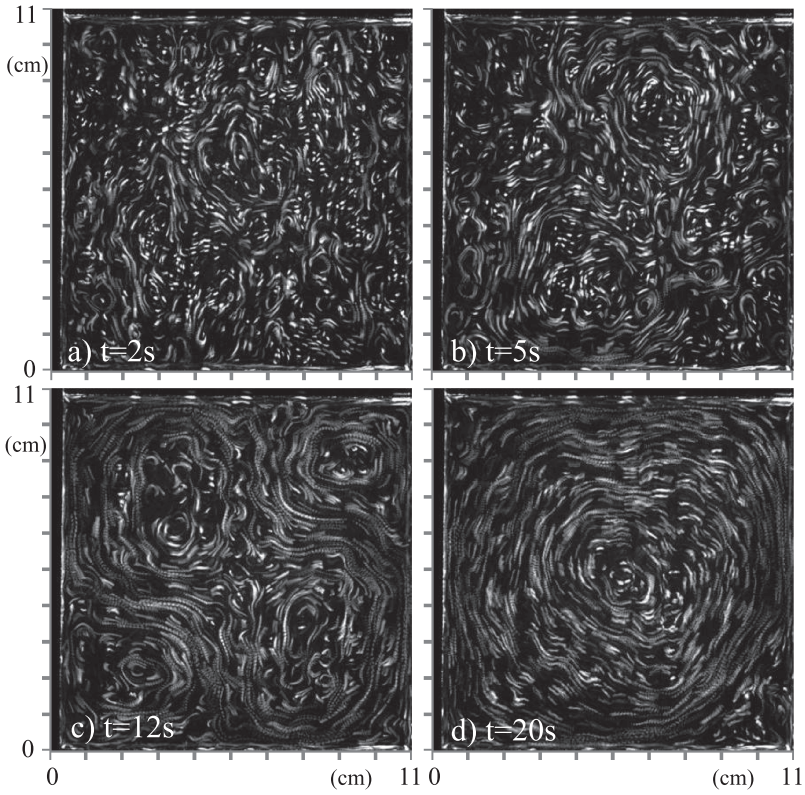

FIG. 8. Generation of a coherent vortex, or spectral condensate, over the entire container in Faraday wave driven turbulence. Temporal evolution of particle streaks on the surface of Faraday waves at (a) t = 2 s, (b) t = 5 s, (c) t = 12 s, and (d) t = 20 s after the wave appearance. Experimental parameters are f_s = 39 Hz and $a = 0.3g$.

were conducted in thin fluid layers (i.e., thickness of the water smaller than the Faraday wavelength) and emphasis was put on the small amplitude of the waves. However, the generation of Faraday wave driven turbulence (FWT) was later confirmed to exist in experiments in deep water and steep waves,[26,29] a configuration that is seemingly unsuitable for 2D turbulence.

Figure 7 shows measurements performed on FWT. In Fig. 7(a), the kinetic energy spectra of the flow at $f_s = 60$ Hz are shown with the corresponding power spectra of the surface wave elevation in Fig. 7(b). While the wave elevation spectra are localised around $k_w \approx 800$ rad/m, the kinetic energy spectra of the flows show a scaling of $E_k \sim k^{-5/3}$, consistent with a 2D inverse energy cascade range.[15,30,31] The energy seems to be injected into the system at half the wavelength, i.e., $k_f \approx 2\pi/(\lambda/2)$, where $\lambda = 2\pi/k_w$ is the Faraday wavelength. Thus, the forcing scale can be controlled by changing the frequency of the shaker as confirmed in Fig. 7(c). The vertical acceleration a controls the level of energy injection into the flow. An increase in a leads to an increase in the total horizontal kinetic energy stored in the inertial range, Fig. 7(a). These observations strongly suggest that energy can be transferred inversely to larger and larger scales in Faraday wave driven flows. This fact is ascertained by measuring the Kolmogorov flux relation. The third-order structure function measured in FWT is shown in Fig. 7(d). It uncovers the presence of an inverse energy cascade for which S_3 is a positive linear function of r, from 0.0075 m to 0.05 m.

The existence of the inverse energy cascade in a bounded flow is a prerequisite for spectral condensation, i.e., the accumulation of the turbulence energy at the box size. In Ref. 26, it was reported that Faraday flows can self-organize into a large coherent vortex at the container scale, as shown in Fig. 8. The sequence of images illustrates the generation of a condensate from initially small-scale vortices [Fig. 8(a)] to a wide hierarchy of scales [Fig. 8(b)], which ultimately produces a large coherent vortex occupying the entire box [Fig. 8(d)].

Until recently, what remained unknown is how and why waves produce 2D turbulence, in particular, how the energy is injected into horizontal flows from vertical oscillations, and why it is injected in a narrow range of scales leaving it to turbulence to spread this energy over a broad inertial interval. In Ref. 29, some of these shortcomings were addressed. It was shown that Faraday waves can produce a lattice of counter-rotating vortices [see Fig. 9(a)] which is the fuel of the 2D turbulent flow. The characteristic scale of these vortices corresponds to half the Faraday wavelength. It gives an intermediate scale for the injection of energy.

In a similar vein, the generation of stable horizontal vortices has been investigated recently in small amplitude standing waves produced by two orthogonal paddles that oscillate horizontally.[54] By tuning the temporal phase of the two orthogonal paddles, it was shown that a periodic pattern of rotating waves can be created. On the fluid surface, such waves rotate within half-wavelength cells. Those waves possess local angular momentum that is transferred to the matter. This mechanism produces particle trajectories in the form of a spatially periodic lattice of vortices as shown in Fig. 9(b). These experiments prove that the deformation of a fluid interface is a powerful and versatile way for vorticity creation in a 2D flow.[55–57]

Clearly the mechanism of flow generation by Faraday waves or nonlinear waves in general needs to be further investigated.[58] Several nonlinear models based on potential or viscous flows near a free surface have been proposed.[52,55,59–61] An interesting path could be related to the Stokes drift induced by the variation of the temporal phase of 2D quasi-standing waves as shown in Fig. 9(b).[54] In that respect, the emergence of disorder in Faraday waves has recently been related to phase instability.[62]

VII. COMPRESSIBILITY OF EMT AND FWT

Faraday flows are indisputably three-dimensional (Fig. 10). Due to the vertical wave oscillations, the divergence computed on the *horizontal* components of the velocity field is clearly non-zero when measured on the time scale of a wave period. The 2D turbulence theory assumption of divergence-free flows is thus violated at this time scale. In this section, we investigate the compressibility of the horizontal velocity field of both EMT and FWT, in particular, its time dependence.

We quantify the divergence of the horizontal velocity field by using the 2D local compressibility parameter $C(x, y)$ and its spatial average C, defined as[63]

$$C(x,y) = \frac{\left\langle (\partial_x v_x + \partial_y v_y)^2 \right\rangle_{T_{av}}}{\langle (\partial_x v_x)^2 + (\partial_x v_y)^2 + (\partial_y v_x)^2 + (\partial_y v_y)^2 \rangle_{T_{av}}}, \quad (1)$$

$$C = \langle C(x,y) \rangle_{x,y}, \quad (2)$$

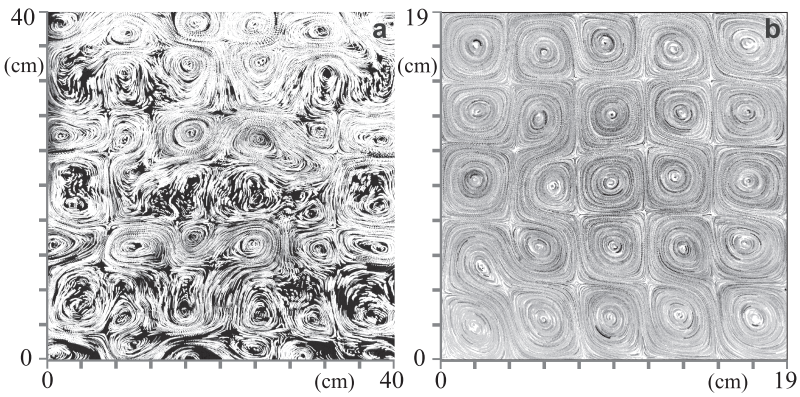

FIG. 9. (a) Surface particle streaks in the initial stage of the flow driven by Faraday waves excited at the water surface at $f_s = 10$ Hz and $a = 0.04g$ in a 40×40 cm^2 square container. (b) Surface particle streaks measured in a standing wave field produced in a square container. The waves are produced by two orthogonal paddles that oscillate horizontally at $f = 4.58$ Hz. The relative temporal phase between the paddles is set to 90°.

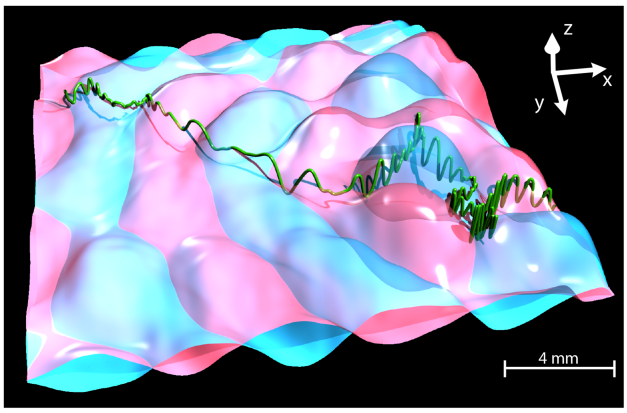

FIG. 10. Perspective view of a three-dimensional particle trajectory followed for 1.6 s at a frame rate of 587 frames/s in a wave field parametrically excited at $a = 1.6g$ and $f_s = 60$ Hz. Pink and blue wave fields correspond to two consecutive phase extrema of the waves that are separated in time by one period of the shaker oscillation (Faraday waves are parametrically excited waves).[29]

where v_x, v_y are the two-dimensional velocity components at the surface. $\langle\cdots\rangle_{x,y}$ denotes average over the 2D surface, and $\langle\cdots\rangle_{T_{av}}$ denotes averaging over time T_{av}.

The meaning of the compressibility parameter C can be illustrated by using simulated velocity fields. For that purpose, we numerically generate two ideal antagonistic flows: a pure solenoidal velocity field in which 2D divergence is everywhere zero [Fig. 11(a)] and a flow produced by a periodic array of source and sink points in the plane [Fig. 11(b)]. The first one is an ideal 2D flow, while the latter is a synthetic way to model 3D effects in a 2D velocity field. For the divergence-free flow, the compressibility parameter $C(x, y)$ is zero in every point. For the source/sink velocity field, the corresponding local $C(x, y)$ parameter shows strong spatial variations taking values from 0 to 2 [Fig. 11(b)]. The local compressibility is extremal, equal to 2, at the location of the source/sink points. The spatial average gives $C = 0.5$. When floating particles are placed into such a flow and initially uniformly distributed over the surface, they will eventually gather at the sinks and flee the sources. In a sense, floating particles on the surface probe the compressibility of the horizontal velocity field. We can use the parameter C to characterise the dimensionality of the flow. The lower the value, the better the 2D approximation for an experimental flow.

The compressibility parameter computed in the EMT double-layer configuration is shown in Fig. 11(c). For experiments at a current over the range $I = (0.2–1)$A, the kinetic energy of the flows increases from 7×10^{-6} m^2/s^2 to 3.6×10^{-5} m^2/s^2. The compressibility parameter C of the flows stays almost constant at a low value of 0.1. The parameter C is independent of the averaging time T_{av} in the EMT experiments, as shown in Fig. 11(d).

In the Faraday wave experiments, the velocity field possesses a vertical component because the wave height oscillates vertically during one Faraday period. This vertical oscillation generates a non-zero compressibility of the horizontal velocity field. These effects are reflected in the importance of the averaging time T_{av} for the calculation of C in FWT. In the FWT experiments [Fig. 11(d)], C takes a value as large as 0.5 when it is not time averaged. When averaged over a couple of Faraday wave periods, C quickly collapses to small values. Quantitatively, C decreases to ~0.1 when averaged over 4 wave periods.

This is an important result: the parameter C averaged over few wave periods in FWT takes a value similar to that measured in double-layer EMT, which is widely accepted as a

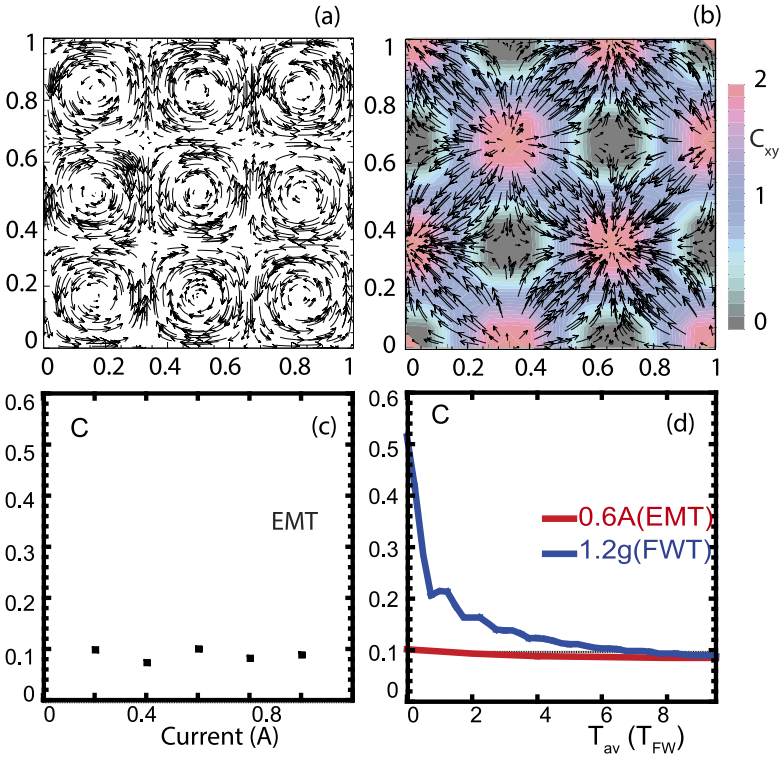

FIG. 11. (a) Velocity field of a pure solenoidal flow. (b) Velocity field of a flow generated by a periodic array of sources and sinks, and its associated compressibility map $C(x, y)$. Compressibility parameter C measured (c) at various flow kinetic energies in the double-layer EMT experiments, and (d) in the double-layer EMT experiments and in the FWT for different integration times T_{av} expressed in wave periods T_{FW}.

good laboratory model of 2D flows. This confirms the quasi-2D and quasi-incompressible nature of the slow (compared to the wave frequency) horizontal flow produced by the Faraday waves. Moreover we also note that our floating tracers stay homogeneously distributed over the water surface perturbed by Faraday waves. This is strong evidence that the 2D flow generated by the waves can be considered as incompressible since a compressible surface flow would induce substantial floater clustering. Indeed in Refs. 63–65, it was shown experimentally that floaters driven by an underlying 3D turbulence form massive ribbon-like clusters and their motion at the fluid surface exhibits properties of a compressible fluid (in such flows, it was reported that $C \approx 0.5$). In the same vein, the dimensionality of Faraday flows has been indirectly tackled in a study of the Belousov-Zhabotinsky chemical reaction in the presence of such flows. The generation of spiral and target patterns was reported, a phenomenon that only occurs in two-dimensional systems.[27]

VIII. WAVE DYNAMICS—2D TURBULENCE COUPLING IN FWT

In this part, we take advantage of recent experimental advances in the generation of Faraday wave driven flows to compare simultaneously the motion of the waves with that of the particles of which they are comprised.[66]

It has been shown that Faraday waves can be considered as an assembly of oscillating solitons or oscillons.[35,36] A method has been developed to track the horizontal motion of an individual oscillon over time [Fig. 12(a)].[36,66] This trajectory based representation of the wave motion can be understood as a characterization of the horizontal motion of the local wave phase. The trajectories of several oscillons followed for 20 Faraday periods are shown in Figs. 12(b) and 12(c) for two different accelerations. First, it can be seen that the oscillons keep relatively well defined positions on a lattice pattern. As a consequence, the wavenumber spectra for the wave elevation

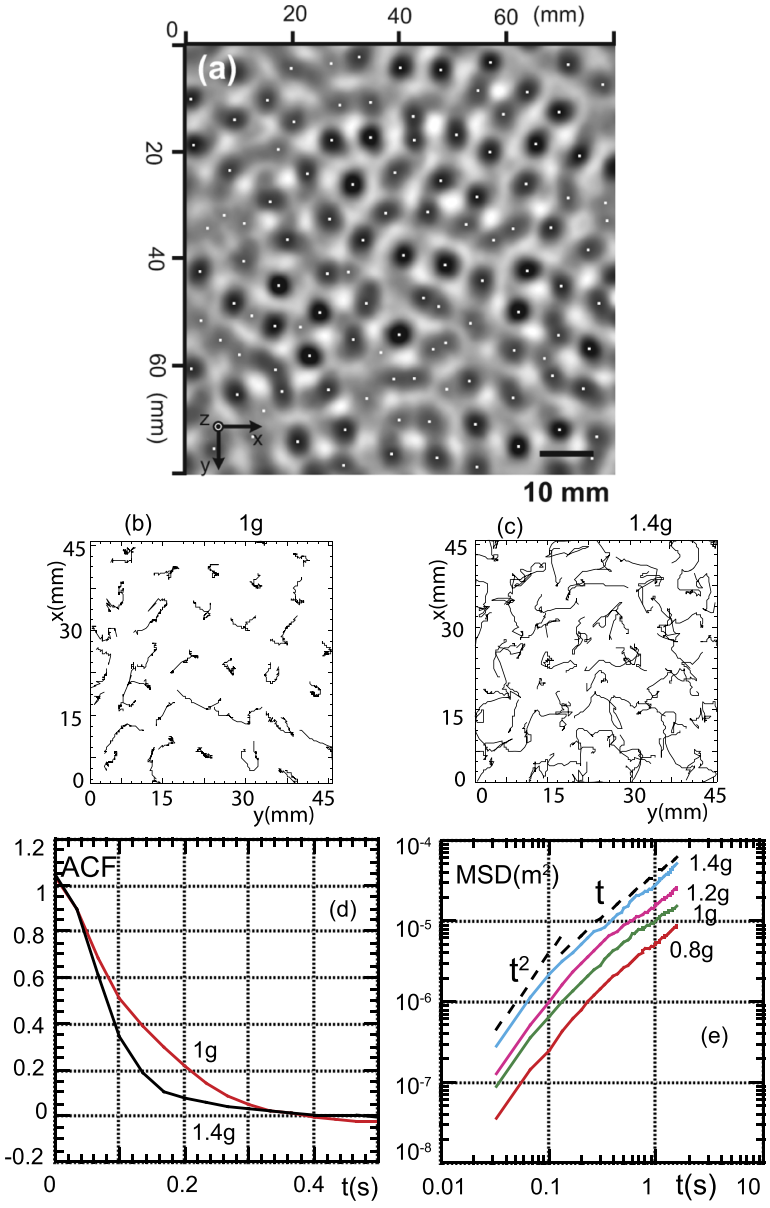

FIG. 12. (a) Top view of Faraday waves using the diffusive light imaging technique. Peaks and troughs appear as dark and white blobs. Local wave maxima are detected (white dots within dark blobs) and their motion is tracked using PTV techniques. [(b) and (c)] Trajectories of oscillons tracked for 20 Faraday wave periods at (b) $a = 1g$ and (c) $a = 1.4g$ with $f_s = 60$ Hz. (d) Autocorrelation function of the oscillon velocity and (e) mean-square-displacement (MSD) of the oscillons.

remains peaked even at high vertical acceleration as shown in Fig. 7(b). Second, the oscillons move randomly in the x-y plane. The memory loss associated with their random motion is quantified by the autocorrelation function of their velocity. Figure 12(d) shows that this function is decreasing and integrable, which leads to a finite autocorrelation time ($T_{osc} \approx 0.15$ s). As a consequence, the mean-square-displacement (MSD) of the oscillon from their initial positions becomes diffusive at times longer than T_{osc} [Fig. 12(e)].

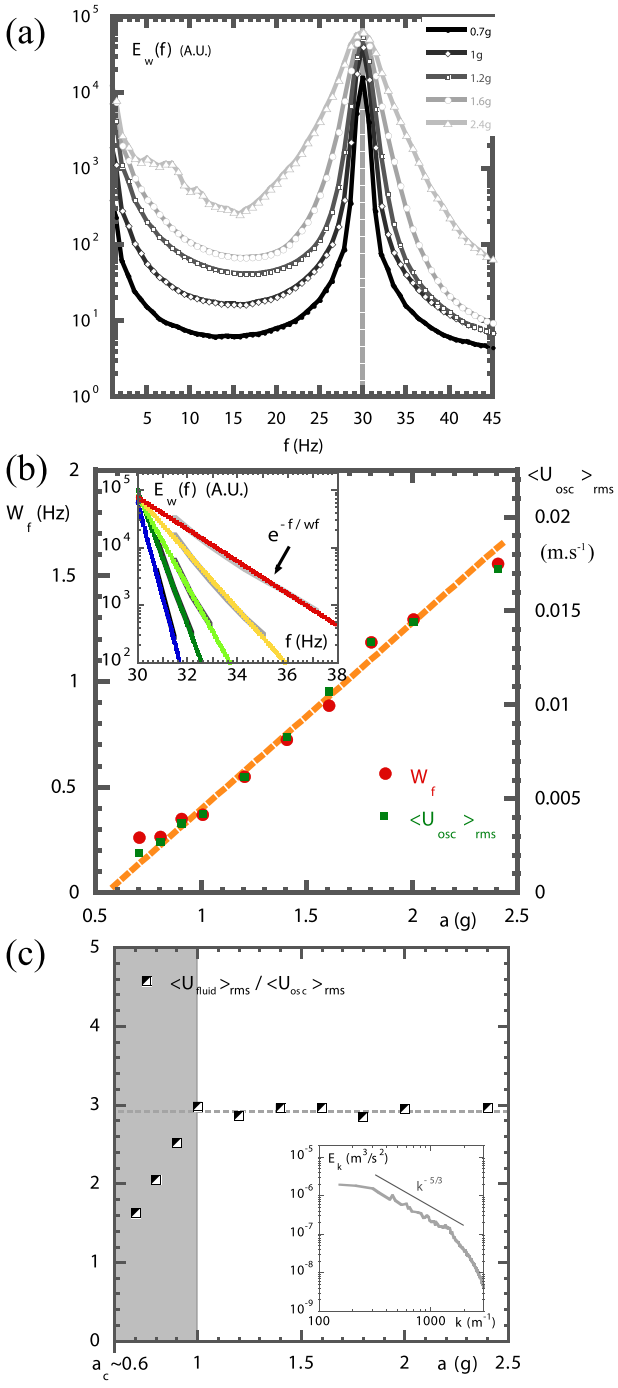

FIG. 13. (a) Frequency power spectra of the Faraday wave elevation at different vertical accelerations a for $f_s = 60$ Hz. (b) Spectral width w_f of the 30 Hz subharmonics [shown in (a)] and oscillon velocity fluctuations $\langle U_{osc}\rangle_{rms}$ versus a. Inset: Close-up on the spectral broadening of the subharmonic at 30 Hz. The lines correspond to exponential fits $exp(-f/w_f)$. (c) Ratio of the rms value of the fluid particle velocity fluctuations $\langle U_{fluid}\rangle_{rms}$ over the oscillon velocity fluctuations $\langle U_{osc}\rangle_{rms}$ versus a. Inset: Wave number spectrum of the horizontal kinetic energy of the fluid particle at $a = 1.6g$.

Faraday waves are often described in terms of the frequency power spectrum of the wave elevation measured at a given point in space by using capacitive measurements or laser reflection techniques. Since Faraday waves are parametrically excited, the main component of their frequency spectra is subharmonic for moderate vertical acceleration.[67] Figure 13(a) shows a close-up on the subharmonic component of such spectra measured for five different accelerations a at $f_s = 60$ Hz. The sub-harmonic broadens with the increase in a and exhibits pronounced exponential tails $\exp(-f/w_f)$ [inset of Fig. 13(b)]. The origin of this exponential decay was discussed in Ref. 35. It is related to the spatial shape of the oscillon which is described by $h(x) \approx \mathrm{sech}(ax)$. The spectral broadening can be characterized by the parameter w_f. Figure 13(b) shows that the behaviour of w_f as a function of a is correlated with that of the oscillon horizontal velocity fluctuations $\langle U_{osc}\rangle_{rms}$. Both quantities scale linearly with the acceleration a.

This result suggests an interesting interpretation of the frequency power spectrum of the Faraday waves. The frequency spectrum is measured locally in space. Therefore the slow random walk of oscillons ($T_{osc} \approx 0.15$ s) about this observation point in the horizontal plane should lead to the broadening of the frequency spectrum by a random Doppler shift. Since the wavenumber spectra of Faraday waves stay peaked at $k_w = 2\pi/\lambda$ [see Fig. 7(b)], such *thermal* broadening should be given by $\triangle f_{th} = \langle U_{osc}\rangle_{rms}/\lambda$. In Ref. 66, the relevance of this interpretation was proven, and it was shown that indeed $w_f \approx \triangle f_{th}$.

In the same study, the motion of fluid particles on the water surface was compared with the motion of oscillons. Figure 13(c) shows that the rms fluid particle velocity $\langle U_{fluid}\rangle_{rms}$ is correlated to the oscillon velocity fluctuations $\langle U_{osc}\rangle_{rms}$ over a broad range of accelerations. $\langle U_{fluid}\rangle_{rms}$ is directly connected to the amount of energy stored in the cascade inertial range [Inset Fig. 13(c)]. These results suggest that 2D turbulence is the driving force behind both the randomization of the oscillon motion and the resulting broadening of the wave frequency spectra. In Ref. 68, it was shown that the suppression of 2D turbulence by the addition of proteins indeed coincides with disorder-order transition in the wave lattice. The coupling between wave motion and 2D hydrodynamic turbulence demonstrated here offers new perspectives for predicting complex fluid transport from the knowledge of wave field spectra and vice versa.

IX. CONCLUSIONS

This paper reviewed recent advances on the emergence of 2D turbulence in 3D flows. Two systems were discussed: flows driven electromagnetically in thick fluid layers and the recently discovered Faraday wave driven flows. In the first system, a main result concerns the interaction of 2D turbulence with a large-scale flow. It was shown how a large-scale vortex and small-scale turbulence conspire to provide for an upscale energy cascade in thick layers. More precisely, these experiments reveal that a large-scale vortex can secure its energy

supply by suppressing vertical motions. In the case of Faraday wave driven flows, though energy is injected into the vertical motion of a liquid, it is converted into turbulent horizontal fluid motion via the generation and interaction of surface vortices. In this system, spectral condensation has recently been observed, and a coupling between wave disorder and 2D hydrodynamic turbulence was discovered.

We started this review by asking if it is possible to create 2D turbulence in experiments. Recent advances on the topic have been surprising. However, at the end of the 1980 review on 2D turbulence,[69] Kraichnan and Montgomery remarked "In some cases, the idealised theory may be more valid in providing a language for discussion rather than a true explanation." The systems discussed in this review broaden the use of this language to unexpected domains.

ACKNOWLEDGMENTS

This work was supported by Australian Research Council's Discovery Projects funding scheme (Nos. DP150103468 and DP160100863). H.X. acknowledges support from Australian Research Council's Future Fellowship (No. FT140100067). N.F. acknowledges support from Australian Research Council's DECRA (No. DE160100742). We thank Jie Geng for his contribution on the computation of the compressibility of surface flows. We thank Michael Shats and Horst Punzmann for countless discussions and their invaluable support.

[1] R. Kraichnan, "Inertial ranges in two-dimensional turbulence," Phys. Fluids **10**, 1417 (1967).
[2] M. Hossain, W. H. Matthaeus, and D. Montgomery, "Long-time states of inverse cascades in the presence of a maximum length scale," J. Plasma Phys. **30**, 479 (1983).
[3] L. Smith and V. Yakhot, "Bose condensation and small-scale structure generation in a random force driven 2D turbulence," Phys. Rev. Lett. **71**, 352 (1993).
[4] L. Smith and V. Yakhot, "Finite-size effects in forced two-dimensional turbulence," J. Fluid Mech. **274**, 115 (1994).
[5] T. Dubos, A. Babiano, J. Paret, and P. Tabeling, "Intermittency and coherent structures in the two-dimensional inverse energy cascade: Comparing numerical and laboratory experiments," Phys. Rev. E **64**, 036302 (2001).
[6] D. Molenaar, H. J. H. Clercx, and G. J. F. van Heijst, "Angular momentum of forced 2D turbulence in a square no-slip domain," Phys. D **196**, 329 (2004).
[7] M. Chertkov, C. Connaughton, I. Kolokolov, and V. Lebedev, "Dynamics of energy condensation in two-dimensional turbulence," Phys. Rev. Lett. **99**, 084501 (2007).
[8] J. Sommeria, "Experimental study of the two-dimensional inverse energy cascade in a square box," J. Fluid Mech. **170**, 139 (1986).
[9] J. Paret and P. Tabeling, "Experimental observation of the two-dimensional inverse energy cascade," Phys. Rev. Lett. **79**, 4162 (1997).
[10] J. Paret and P. Tabeling, "Intermittency in the two-dimensional inverse cascade of energy: Experimental observations," Phys. Fluids **10**, 3126 (1998).
[11] M. G. Shats, H. Xia, and H. Punzmann, "Spectral condensation of turbulence in plasmas and fluids and its role in low-to-high phase transitions in toroidal plasma," Phys. Rev. E **71**, 046409 (2005).
[12] S. Chen, R. E. Ecke, G. L. Eyink, M. Rivera, M. Wan, and M. Xiao, "Physical mechanism of the two-dimensional inverse energy cascade," Phys. Rev. Lett. **96**, 084502 (2006).
[13] M. Shats, H. Xia, H. Punzmann, and G. Falkovich, "Suppression of turbulence by self-generated and imposed mean flow," Phys. Rev. Lett. **99**, 164502 (2007).
[14] H. Xia, H. Punzmann, G. Falkovich, and M. G. Shats, "Turbulence-condensate interaction in two dimensions," Phys. Rev. Lett. **101**, 194504 (2008).
[15] H. Xia, M. Shats, and G. Falkovich, "Spectrally condensed turbulence in thin layers," Phys. Fluids **21**, 125101 (2009).
[16] N. T. Ouellette, "Turbulence in two dimensions," Phys. Today **65**(5), 68 (2012).
[17] M. Shats, D. Byrne, and H. Xia, "Turbulence decay rate as a measure of flow dimensionality," Phys. Rev. Lett. **105**, 264501 (2010).
[18] Y. Couder, J. M. Chomaz, and M. Rabaud, "On the hydrodynamics of soap films," Phys. D **37**, 384 (1989).
[19] H. Kellay, X.-I. Wu, and W. I. Goldburg, "Experiments with turbulent soap films," Phys. Rev. Lett. **74**, 3975 (1995).
[20] T. Tran *et al.*, "Macroscopic effects of the spectral structure in turbulent flows," Nat. Phys. **6**, 438 (2010).
[21] H. Kellay, T. Tran, W. Goldburg, N. Goldenfield, G. Gioia, and P. Chakraborty, "Testing a missing spectral link in turbulence," Phys. Rev. Lett. **109**, 254502 (2012).
[22] H. Kellay and W. Goldburg, "Two-dimensional turbulence: A review of some recent experiments," Rep. Prog. Phys. **65**, 845 (2002).
[23] D. Byrne, H. Xia, and M. Shats, "Robust inverse energy cascade and turbulence structure in three-dimensional layers of fluid," Phys. Fluids **23**, 095109 (2011).
[24] H. Xia, D. Byrne, G. Falkovich, and M. Shats, "Upscale energy transfer in thick turbulent fluid layers," Nat. Phys. **7**, 321 (2011).
[25] A. von Kameke, F. Huhn, G. Fernandez-Garcia, A. P. Munuzuri, and V. Perez-Munuzuri, "Double cascade turbulence and Richardson dispersion in a horizontal fluid flow induced by Faraday waves," Phys. Rev. Lett. **107**, 074502 (2011).
[26] N. Francois, H. Xia, H. Punzmann, and M. Shats, "Inverse energy cascade and emergence of large coherent vortices in turbulence driven by Faraday waves," Phys. Rev. Lett. **110**, 194501 (2013).
[27] A. von Kameke, F. Huhn, A. P. Muñuzuri, and V. Pérez-Muñuzuri, "Measurement of large spiral and target waves in chemical reaction-diffusion-advection systems: Turbulent diffusion enhances pattern formation," Phys. Rev. Lett. **110**, 088302 (2013).
[28] A. von Kameke, F. Huhn, G. Fernandez-Garcia, A. P. Munuzuri, and V. Perez-Munuzuri, "Propagation of a chemical wave front in a quasi-two-dimensional superdiffusive flow," Phys. Rev. E **81**, 066211 (2011).
[29] N. Francois, H. Xia, H. Punzmann, S. Ramsden, and M. Shats, "Three-dimensional fluid motion in Faraday waves: Creation of vorticity and generation of two-dimensional turbulence," Phys. Rev. X **4**, 021021 (2014).
[30] H. Xia, N. Francois, H. Punzmann, and M. Shats, "Lagrangian scale of particle dispersion in turbulence," Nat. Commun. **4**, 3013 (2013).
[31] H. Xia, N. Francois, H. Punzmann, and M. Shats, "Taylor particle dispersion during transition to fully developed two-dimensional turbulence," Phys. Rev. Lett. **112**, 104501 (2014).
[32] H. Xu *et al.*, "Flight-crash events in turbulence," Proc. Natl. Acad. Sci. U. S. A. **111**, 7558 (2014).
[33] N. Francois, H. Xia, H. Punzmann, B. Faber, and M. Shats, "Braid entropy of two-dimensional turbulence," Sci. Rep. **5**, 18564 (2015).
[34] G. Boffetta and R. Ecke, "Two-dimensional turbulence," Annu. Rev. Fluid Mech. **44**, 427 (2012).
[35] M. Shats, H. Xia, and H. Punzmann, "Parametrically excited water surface ripples as ensembles of oscillons," Phys. Rev. Lett. **108**, 034502 (2012).
[36] H. Xia, T. Maimbourg, H. Punzmann, and M. Shats, "Oscillon dynamics and rogue wave generation in Faraday surface ripples," Phys. Rev. Lett. **109**, 114502 (2012).
[37] A. Celani, S. Musacchio, and D. Vincenzi, "Turbulence in more than two and less than three dimensions," Phys. Rev. Lett. **104**, 184506 (2010).
[38] G. Boffetta and A. Mazzino, "Incompressible Rayleigh-Taylor turbulence," Ann. Rev. Fluid Mech. **49**, 119–143 (2017).
[39] G. D. Nastrom, K. S. Gage, and W. H. Jasperson, "Kinetic energy spectrum of large- and mesoscale atmospheric processes," Nature **310**, 36 (1984).
[40] K. S. Gage and G. D. Nastrom, "Theoretical interpretation of atmospheric wavenumber spectra of wind and temperature observed by commercial aircraft during GASP," J. Atmos. Sci. **43**, 729 (1986).
[41] D. K. Lilly, "Two-dimensional turbulence generated by energy sources at two scales," J. Atmos. Sci. **43**, 2026 (1989).
[42] E. Lindborg, "Can the atmospheric kinetic energy spectrum be explained by two-dimensional turbulence?," J. Fluid Mech. **388**, 259 (1999).
[43] J. Y. N. Cho and E. Lindborg, "Horizontal velocity structure functions in the upper troposphere and lower stratosphere: 1. Observations," J. Geophys. Res. **106**, 10223, doi:10.1029/2000JD900814 (2001).

[44]D. Byrne and J. Zhang, "Height-dependent transition from 3-D to 2-D turbulence in the hurricane boundary layer," Geophys. Res. Lett. **40**, 1439, doi:10.1002/grl.50335 (2013).
[45]S. Douady and S. Fauve, "Pattern selection in Faraday instability," Europhys. Lett. **6**, 221 (1988).
[46]W. S. Edwards and S. Fauve, "Patterns and quasi-patterns in the Faraday experiment," J. Fluid Mech. **278**, 123 (1994).
[47]A. Kudrolli and J. P. Gollub, "Patterns and spatiotemporal chaos in parametrically forced surface waves: A systematic survey at large aspect ratio," Phys. D **97**, 133 (1996).
[48]J. Wu, R. Keolian, and I. Rudnick, "Observation of a nonpropagating hydrodynamic soliton," Phys. Rev. Lett. **52**, 1421 (1984).
[49]O. Lioubashevski, H. Arbell, and J. Fineberg, "Dissipative solitary states in driven surface waves," Phys. Rev. Lett. **76**, 3959 (1996).
[50]M. Shats, H. Punzmann, and H. Xia, "Capillary rogue waves," Phys. Rev. Lett. **104**, 104503 (2010).
[51]R. Ramshankar, D. Berlin, and J. P. Gollub, "Transport by capillary waves. Part I. Particle trajectories," Phys. Fluids A **2**, 1955 (1990).
[52]O. N. Mesquita, S. Kane, and J. P. Gollub, "Transport by capillary waves: Fluctuating Stokes drift," Phys. Fluids A **45**, 3700 (1992).
[53]A. E. Hansen *et al.*, "Fractal particle trajectories in capillary waves: Imprint of wavelength," Phys. Rev. Lett. **79**, 1845 (1997).
[54]N. Francois, H. Xia, H. Punzmann, F. W. Fontana, and M. Shats, "Wave-based liquid-interface metamaterials," Nat. Commun. **7**, 14325 (2017).
[55]Z. C. Feng and S. Wiggins, "Fluid particle dynamics and Stokes drift in gravity and capillary waves generated by the Faraday instability," Adv. Nonlinear Dyn. **8**, 141–160 (1995).
[56]P. G. Saffman, *Vortex Dynamics* (Cambridge University Press, 1992).
[57]M. S. Longuet-Higgins, "Vorticity and curvature at a free surface," J. Fluid Mech. **356**, 149 (1998).
[58]H. Punzmann, N. Francois, H. Xia, G. Falkovich, and M. Shats, "Generation and reversal of surface flows by propagating waves," Nat. Phys. **10**, 658 (2014).
[59]M. Umeki, "Particle transport by angular momentum on three-dimensional standing surface waves," Phys. Rev. Lett. **67**, 2650–2653 (1991).
[60]S. V. Filatov *et al.*, "Non-linear generation of vorticity by surface waves," Phys. Rev. Lett. **116**, 054501 (2016).
[61]E. Martin, C. Martel, and J. M. Vega, "Drift instability of standing Faraday waves," J. Fluid Mech. **467**, 57 (2002).
[62]I. Shani, G. Cohen, and J. Fineberg, "Localized instability on the route to disorder in Faraday waves," Phys. Rev. Lett. **104**, 184507 (2010).
[63]J. R. Cressman, J. Davoudi, W. I. Goldburg, and J. Schumacher, "Eulerian and Lagrangian studies in surface flow turbulence," New J. Phys. **6**, 53 (2004).
[64]J. Larkin, M. M. Bandi, A. Pumir, and W. I. Goldburg, "Power-law distributions of particle concentration in free-surface flows," Phys. Rev. E **80**, 066301 (2009).
[65]M. M. Bandi, W. I. Goldburg, and J. R. Cressman, Jr., "Measurement of entropy production rate in compressible turbulence," Europhys. Lett. **76**, 595 (2006).
[66]N. Francois, H. Xia, H. Punzmann, and M. Shats, "Wave-particle interaction in the Faraday waves," Euro. Phys. J. E **38**, 106 (2015).
[67]H. Xia, M. Shats, and H. Punzmann, "Modulation instability and capillary wave turbulence," Europhys. Lett. **91**, 14002 (2010).
[68]N. Francois, H. Xia, H. Punzmann, T. Combriat, and M. Shats, "Inhibition of wave-driven two-dimensional turbulence by viscoelastic films of proteins," Phys. Rev. E **92**, 023027 (2015).
[69]R. Kraichnan and D. Montgomery, "Two-dimensional turbulence," Rep. Prog. Phys. **43**, 547 (1980).